Selective measurement of charge dynamics in an ensemble of nitrogen-vacancy centers in nanodiamond and bulk diamond

R. Giri,[1,*] C. Dorigoni,[1] S. Tambalo,[1] F. Gorrini,[1] and A. Bifone[1,2]

[1]*Center for Neuroscience and Cognitive Systems, Istituto Italiano di Tecnologia, Corso Bettini 31, Rovereto 38068, Italy*

[2]*Department of Molecular Biotechnology and Health Sciences, University of Turin, Via Verdi 8, Turin 10124, Italy*

(Received 14 March 2019; published 26 April 2019)

Nitrogen-vacancy (NV) centers in diamond have attracted considerable interest in sensing of weak magnetic fields, such as those created by biological systems. Detecting such feeble signals requires near-surface NV centers, to reduce the distance between NVs and sources. Moreover, dense ensembles of NVs are highly desirable to reduce measurement time. However, robust charge-state switching is often observed in these systems, resulting in a complex interplay between charge and spin dynamics that can reduce the attainable level of spin polarization, and consequently, sensitivity. Understanding the mechanisms behind charge-state switching is, therefore, crucial to developing NV-based sensors. Here, we demonstrate a method to selectively measure charge dynamics in an ensemble of NVs by quenching the spin polarization using an off-axis magnetic field. Utilizing this technique, we show that, in nanodiamonds, charge-state instability increases with increasing NV density. In the case of bulk single crystal diamond, we show that NV centers located near the surface are more stable in the neutral (NV^0) charge state, while the negatively charged (NV^-) form is more stable in bulk.

DOI: 10.1103/PhysRevB.99.155426

I. INTRODUCTION

The nitrogen-vacancy (NV) center is one of the numerous color centers found in the diamond. It is commonly observed in either the neutral (NV^0) or negatively charged state (NV^-) [1–3]. While the spin state of the negatively charged NV centers can be manipulated with optical and microwave excitation [4], experimental control of the spin state of the NV^0 centers remains elusive, although theoretically possible [5,6]. The electron spin degree of freedom of the NV^- centers has been exploited for potential applications in quantum sensing, nanoscale MRI, and quantum computing [7–10]. Therefore, controlling the charge state of the NV centers is crucial. A stable and well-controlled NV charge state not only improves the sensitivity of detection, but also leads to applications such as sensing of electrochemical potentials [11] and enhanced nuclear spin coherence time [12].

While single isolated NV centers enabled magnetic sensing with nanoscale resolution, ensembles of NV centers are desirable in applications where sensitivity is a critical factor to increase photon counts and reduce measurement time [9]. However, charge-state instability may become acute in the case of dense ensembles of NVs [13]. Various factors, such as nitrogen defects, surface states, vacancies, and other deep-level defects can influence the charge-state stability of the NV centers during initialization as well as in the dark [14–16]. In spite of the detrimental impact of charge-state instability on spin polarization [13,17], and consequently on the sensing capabilities of NV centers, a clear understanding of charge dynamics of NV ensembles is lacking.

Attempts to control the charge states of NVs by manipulating the Fermi level are reported in the literature [11,18–22]. It was demonstrated that an ensemble of NV centers could be stable enough to be used as a charge-based data storage medium [23,24]. Other studies on dense ensembles of NVs and near-surface single NVs reported a strong interplay between charge and spin dynamics during illumination as well as in the dark that can interfere with spin measurements [13,25,26]. Disentangling the two contributions is critical to understand the underlying physical mechanisms, and to enable effective control of charge dynamics in many applications.

Selective measurements of the spin dynamics in the dark were shown to be feasible by removing contributions from recombination as well as ionization of NVs in the dark [26–28]. However, a complementary technique to selectively measure the charge dynamics of NV ensembles is lacking. To this end, pulse sequences involving green and yellow lasers have been proposed [13,15,29], but they are not effective in removing the spin contribution entirely. Studies on the charge dynamics of single NV centers as well as the stochastic change of the charge states under laser illumination have been reported [20,30], but these measurements are not applicable in the case of an NV ensemble. Methods to study charge-state distribution in an NV ensemble have been recently proposed [31]; however, this technique does not allow studying charge dynamics, particularly in the dark.

Here, we note that an off-axis magnetic field (a few degrees off the NV axis) can mix the $m_s = 0$ and $m_s = \pm 1$ spin states of the NV centers, and lead to a reduction of excited state lifetime, fluorescence intensity, as well as electron spin resonance contrast [32,33]. An external magnetic field along the [100] crystal axis makes an equal angle of 54.7° to all

*rakshyakar.giri@iit.it

four NV orientations, and a field around 500 G ∥ [100] could completely mix the spin states resulting in zero spin polarization [33,34].

In this work, we demonstrate this principle in an ensemble of NV centers in nanodiamond powders and in bulk diamond, showing that it is feasible to selectively measure charge-state dynamics of an NV ensemble during laser illumination as well as in the dark. We observed that increasing the strength of the applied magnetic field results in a reduction of the spin polarization during a 532-nm laser illumination. Complete elimination of the spin polarization was achieved at 600 G, revealing pure ionization-recharge dynamics, without any visible impact of the magnetic field in the NV^- and NV^0 populations. We applied this approach to study charge dynamics in nanodiamonds with different densities of NVs, and in bulk single-crystal diamond as a function of the distance of the NVs from the surface.

II. METHODS

The nanodiamond (ND) samples used in this study are uncoated fluorescent nanodiamonds from Bikanta (Berkeley, CA), with nominal diameter 100 nm (FND100). The nanodiamonds are strongly fluorescent due to a high concentration of NVs (≈5 ppm), with each ND containing about 500 NV centers. We deposited the NDs on a cover glass to carry out all the measurements.

We obtained the chemical vapor deposition (CVD) grown single-crystal diamonds used here from Element Six Ltd. One sample (S6) is a single-crystal diamond plate, (100) oriented, with <1 ppm nitrogen. We estimated the concentration of NV centers to be about 0.028 ppm by comparison of the level of fluorescence with a reference sample. The other single-crystal diamond (EG6) is an electronic grade sample, (100) oriented, with nitrogen concentration <5 ppb. The sample has been implanted with ^{15}N ions at 15 keV with a dose of 1×10^{13} ions/cm^2, using an angle of incidence of 7°. Ion average range, calculated by SRIM [35], is about 21 nm. Subsequent annealing in helium gas at 850 °C for 2 h results in near-surface NV centers, which we estimated to be about 2.4 ppb.

We used a home-built confocal microscope [see Fig. 1(a)] equipped with an objective lens of 0.25 NA and operating at room temperature. We used a 532-nm laser for both spin- and charge-state initialization as well as detection. The NV^0 and NV^- centers have zero- phonon lines at 575 and 637 nm, respectively, with broad phonon sidebands [3]. We used a series of bandpass filters to detect fluorescence from the NV^0 and NV^- charge states. A single-photon-counting module (Excelitas, SPCM-AQRH-14-FC) was used to detect the fluorescence. An acousto-optic modulator (AA Optoelectronics, MT 200-A0, 5-VIS) produced the excitation laser pulses, and a programmable transistor-transistor logic pulse generator (Spincore, PulseBlaster ESR-PRO) was used to generate the pulse sequences. A permanent magnet was mounted on a

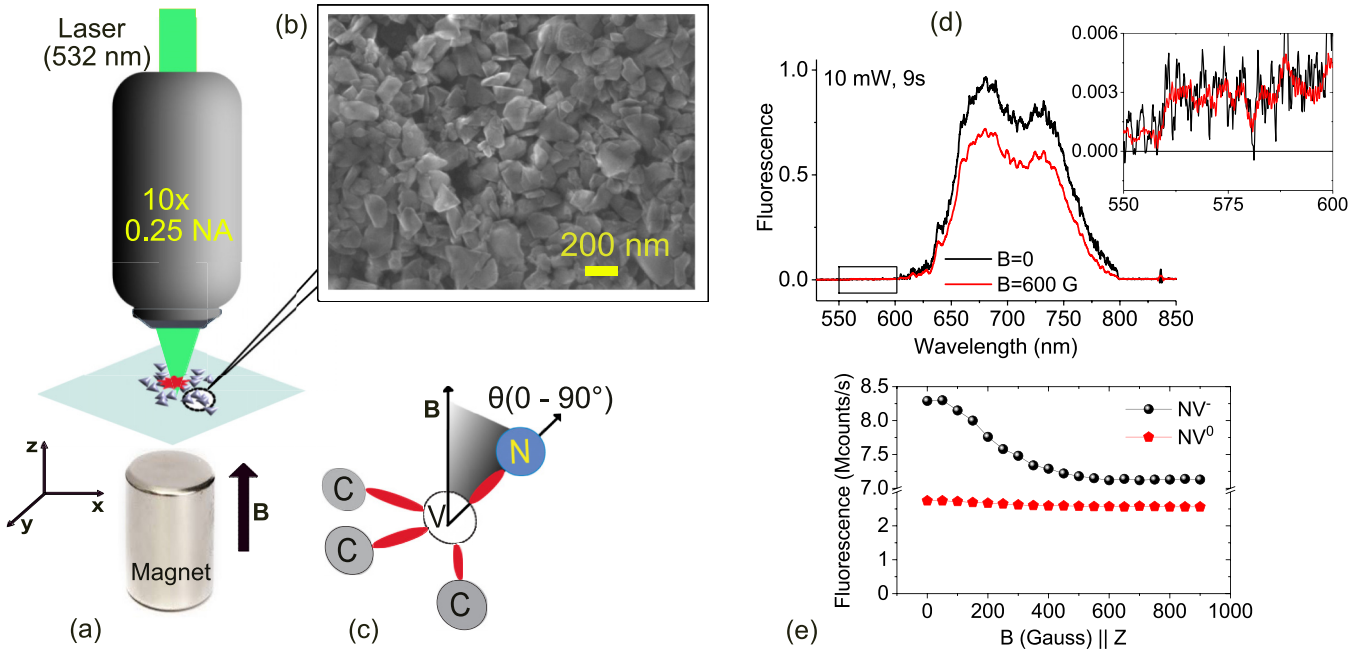

FIG. 1. (a) Schematic of the experimental setup. The nanodiamonds (nominally 100 nm diameter) are deposited on a cover glass, and the green excitation laser was focused on the sample by a 0.25 NA microscope objective. The fluorescence was collected using the same objective, and bandpass filters were used to filter out the fluorescence corresponding to NV^- and NV^0 emission. A permanent magnet placed directly below the sample produced the static magnetic field. (b) SEM image of the NDs deposited on a silicon substrate showing random crystal orientations. (c) The NV defect axes oriented randomly to the applied magnetic field, and the angle θ could range from 0 to 90°. (d) Effect of magnetic field on the fluorescence spectra of the NV ensembles in the nanodiamonds. The inset shows the effect on fluorescence originating from the NV^0 centers. (e) Variation of NV^- and NV^0 fluorescence intensity as a function of external magnetic field, indicating mixing of spin states, but no apparent change in the ionization of the NVs.

linear translation stage to apply a variable static magnetic field along the vertical (z) axis.

III. RESULTS AND DISCUSSION

We show the fluorescence emission spectra of the ensembles of NV centers in the nanodiamond powder sample in Fig. 1(d), obtained by continuously illuminating the sample with a 10-mW laser at 532 nm. The 10-mW laser power used is much weaker than the saturation power (more than 500 mW) for these samples. Only a 532-nm notch filter and 800-nm short pass filters were used for this measurement. The fluorescence in the wavelength range from 550 to 600 nm originates from NV^0 centers, while emission from the NV^- phonon sideband dominates the 650–800 nm region [16,36]. Application of an external magnetic field, **B**, reduced the NV^- fluorescence. However, the NV^0 fluorescence level is hardly affected [inset in Fig. 1(d)]. These results are consistent with previous reports on an ensemble of NV centers in high-pressure high-temperature bulk diamond [16,37].

We also spectrally filtered the NV^0 (550–600 nm) and NV^- (750–800 nm) fluorescence; these narrow bands were chosen to help minimize the signal overlap. Figure 1(e) shows the variation of NV^0 and NV^- fluorescence with increasing **B**. The NV^- fluorescence decreases monotonically with the increase in the strength of **B** and reaches saturation at fields stronger than 500 G. In the case of nanodiamond powder, the crystal orientations are random, and each NV makes a random angle to **B** (Fig. 1). The monotonic decrease of the fluorescence with increasing **B** suggests that $\theta_{\text{avg.}} > 20^\circ$ [34], and is a general indication of sufficient mixing of the $m_s = 0$ and $m_s = \pm 1$ spin states [33,34,38]. However, the NV^0 fluorescence level is not significantly affected by the change in the magnetic field strength (the slight change of intensity could be due to a small overlap of NV^- contribution). These results suggest that the magnetic field quenches only the spin polarization of the NV centers, but does not significantly affect the NV populations in either of the charge states. We note here that contrasting results were obtained in single NV centers in high-purity CVD diamond [39], indicating fundamentally different ionization and recombination mechanisms in NV ensembles.

Next, we demonstrate that an off-axis magnetic field could indeed quench the NV^- spin polarization. We used the nanodiamond powder sample and employed a simple pulse sequence as shown in Fig. 2(a) (upper panel). The laser was off for the initial 5 ms, much longer than the typical T_1-relaxation time in these nanodiamonds, to allow the sample to relax in the dark [38]. Then, we applied a 10-mW laser pulse at 532 nm, well below saturation, and monitored the fluorescence of the NV^- centers (750–800 nm band). We show the time evolution of the fluorescence intensity in Fig. 2(a) (lower panel). At the beginning of the laser pulse, the fluorescence increases until it reaches a maximum and then starts to decay with time. We can interpret the evolution of the curve as

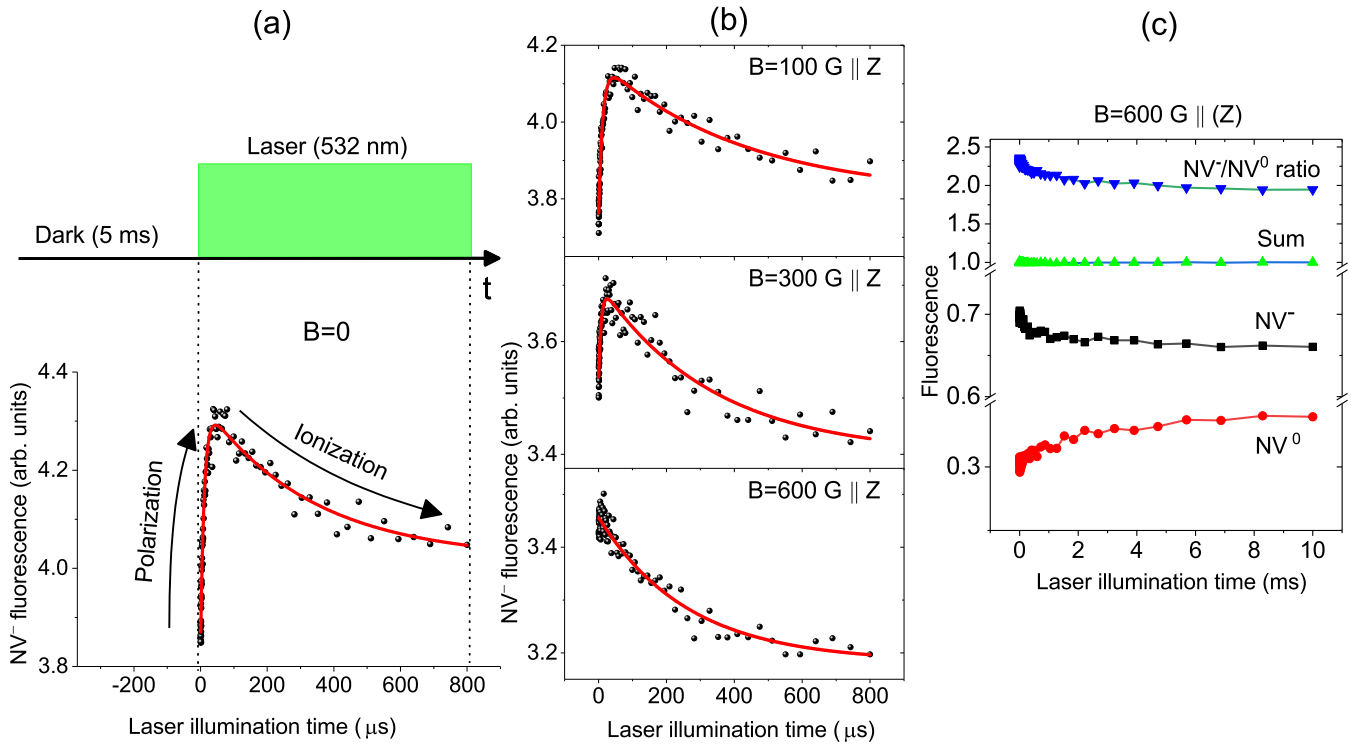

FIG. 2. (a) Pulse sequence used to measure the charge and spin dynamics in the nanodiamond powder during 532-nm laser illumination. The system is allowed to relax for 5 ms in the dark, and the time dependence of the fluorescence intensity is recorded during excitation. The lower panel depicts the time evolution of fluorescence intensity at B = 0, indicating a convolution of spin and charge dynamics. (b) Fluorescence signal temporal evolution for increasing applied field strength, showing a gradual reduction of spin polarization. (c) Complete suppression of spin polarization is obtained at B = 600 G ∥ Z, showing pure charge dynamics: ionization of NV^- centers is paralleled by an increase of NV^0 centers. The red solid lines represent biexponential fits.

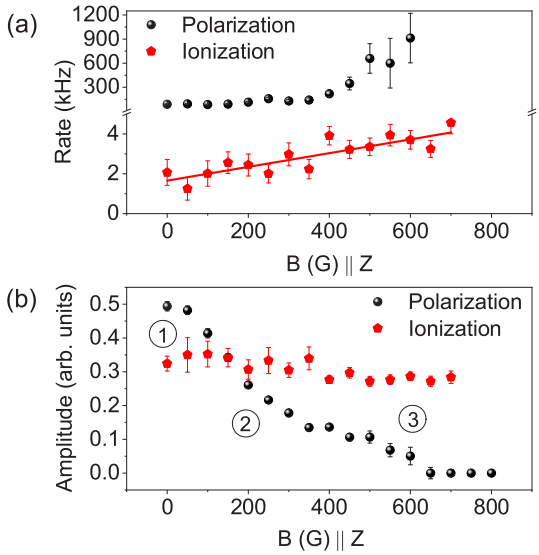

FIG. 3. (a) Rates, and (b) amplitudes of spin polarization and ionization of NVs during 532-nm laser illumination, extracted from biexponential fits of curves as in Fig. 2(b). The red solid line in the upper panel is a linear fit to the data.

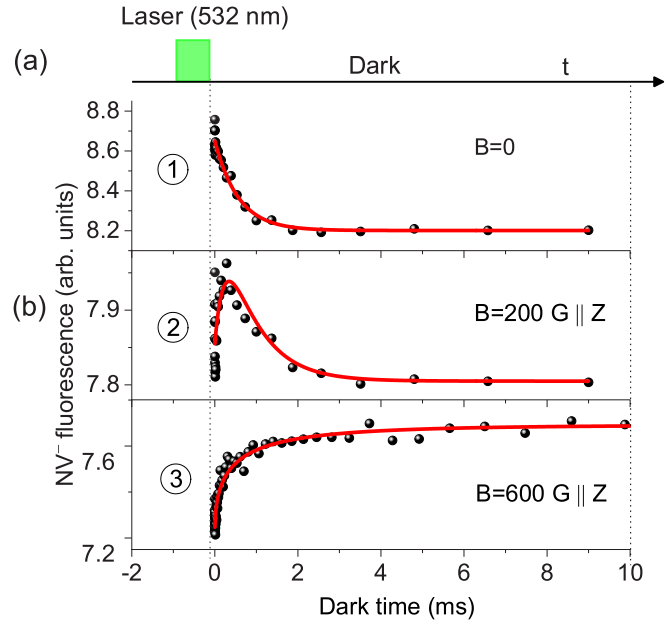

FIG. 4. (a) Pulse sequence used to measure spin-charge dynamics in the dark following green excitation for 1 ms. (b) Fluorescence evolution with dark time for the three regimes marked in Fig. 3(b). Regime 1 ($B = 0$): Charge dynamics is completely masked by spin relaxation in the dark. Regime 2 ($B = 200$ G): Reduction of spin-polarization results in an almost equal spin and charge contribution to the fluorescence evolution in the dark. Regime 3 ($B = 600$ G): Spin polarization vanishes completely, revealing the hidden recharging process of NV centers in the dark.

follows. The laser pulse, due to the Gaussian nature of the excitation spot, polarizes the NDs with a characteristic time that depends on laser power and the intrinsic NV^- spin-relaxation mechanisms. Also, ionization and recombination of the NV centers under green laser illumination are robust in the presence of high defect concentrations such as substitutional nitrogens [14,16,40]. These two competing processes result in the biexponential evolution of the fluorescence during illumination. This interplay between spin and charge dynamics has been thoroughly described in Ref. [25]. As we discussed earlier, an off-axis magnetic field can quench the NV^- spin polarization. If the initial increase of the fluorescence is indeed due to spin polarization, then it should be affected by magnetic fields. Figure 2(b) shows that it is indeed the case. The rising component gets smaller in amplitude with increasing **B**, and at 600 G the fluorescence evolution is dominated by a decaying component corresponding to increasing depletion of the NV^- population by charge transfer. In order to substantiate this interpretation, we monitored the fluorescence of the NV^0 centers (550–600 nm band). The time dependence of the NV^0 fluorescence intensity is symmetric to that of the NV^- fluorescence intensity [Fig. 2(c)]. This indicates that photoionization of NV^- centers increases NV^0 populations which are reflected in their emission intensity [3,14,41,42]. The fluorescence signal is devoid of any contribution from spin polarization, and under this experimental condition, we can selectively explore the charge-state dynamics of the NV centers under green illumination.

We extracted the amplitudes and rates of the two competing processes of charge and spin dynamics during illumination, from the biexponential fits of curves as in Figs. 2(a) and 2(b). The spin-polarization rate and ionization rate as a function of the off-axis magnetic field are plotted in Fig. 3(a). The spin-polarization rate appears to increase as the magnetic field increases until spin-state mixing quenches the polarization completely [black spheres in Fig. 3(a)]. The magnetic field can stimulate the transition from the NV^- excited state to the metastable singlet state, resulting in an increase in the populations in the metastable state [16,37,38], thereby increasing the rate at which the NV^- centers are initialized into the $m_s = 0$ state. However, this process can also induce the ionization of the NV^- centers from the excited state as well as the metastable singlet state through a single-photon ionization process, a process typical of diamonds with high defect concentration [38]. Thus, increasing the magnetic field strength leads to an increased rate of ionization [red hexagons in Fig. 3(a)]. However, the amplitude of the ionization process largely remains unaffected by the magnetic field [red hexagons in Fig. 3(b)], and the only noticeable effect of the magnetic field is a reduction of the amplitude of spin polarization [black spheres in Fig. 3(b)]. Thus, we have three distinct regimes as marked in Fig. 3(b). When no external magnetic field is applied, the spin polarization of the NV^- centers dominates over the ionization process (Regime 1). With an increase in the field strength, spin-state mixing results in a decrease in the amplitude of spin polarization, and at about 200 G, the contributions of spin polarization and ionization are almost equal (Regime 2). Any further increase in field strength results in a situation where the ionization process dominates over spin polarization, and at $B = 600$ G, the spin polarization is suppressed, revealing the dynamics of the ionization process (Regime 3).

We further investigated the spin-charge dynamics in the dark in these three distinct regimes. We used a standard T_1-relaxation pulse sequence as shown in Fig. 4(a). We initialized

the system for 1 ms using a 532-nm laser and monitored the fluorescence evolution in the dark using a 1-μs readout pulse at the same wavelength. For $B = 0$, we observed a simple exponential type decay indicative of spin relaxation in the dark dominating over charge dynamics. The hidden charge dynamics was recently exploited to increase the sensitivity of magnetic noise detection [43], but it could also have a detrimental effect on the spin-relaxation measurements [25,26]. At $B = 200$ G, charge dynamics emerge, as spin-state mixing reduces the amplitude of spin polarization that could be achieved by the laser pulse. The result is a biexponential type decay curve similar to the ones previously reported [25,43]. At $B = 600$ G, as the spin polarization is completely quenched, fluorescence evolution is dictated by charge dynamics in the dark.

Our method also allows estimation of the charge-state distribution of the NV ensemble in the steady state under illumination, as well as in equilibrium in the dark. We can write the time evolution of the fluorescence signal of the NV ensemble [for example, as in Fig. 2(c)] as

$$I^{-}(t) = I^{-}_{\mathrm{eq}}[1 - \alpha e^{-t/T_r}], \tag{1}$$

$$I^{0}(t) = I^{0}_{\mathrm{eq}}[1 + \alpha' e^{-t/T_r}], \tag{2}$$

where I^{-}_{eq} and I^{0}_{eq} are the fluorescence intensity in the steady state/equilibrium of the NV^{-} and NV^{0} centers, respectively. α and α' are the amplitudes of ionization and recombination process, and T_r is the recharging/ionization time. Assuming that the total NV population remains constant, the equilibrium population of the NV^{-} and NV^{0} centers are related as

$$N^{0}_{\mathrm{eq}} = \frac{\alpha}{\alpha'} N^{-}_{\mathrm{eq}} \tag{3}$$

and the relative fractions in equilibrium are

$$\frac{N^{-}_{\mathrm{eq}}}{N_{\mathrm{total}}} = \frac{\alpha'}{\alpha + \alpha'}, \tag{4a}$$

$$\frac{N^{0}_{\mathrm{eq}}}{N_{\mathrm{total}}} = \frac{\alpha}{\alpha + \alpha'}. \tag{4b}$$

Therefore, the ratio of the NV^{-} to NV^{0} population in an NV ensemble at a given time can be written as

$$R \equiv \frac{[NV^{-}]}{[NV^{0}]} = \frac{\alpha}{\alpha'}. \tag{5}$$

We estimated that during the illumination with a 10-mW green laser for 10 ms, the charge-state ratio, R, in the nanodiamonds decreases from 70/30 to 66/34 [Fig. 2(c)]. In the dark, the NV centers recharge, and the charge-state ratio increases from 73/27 to 78/22 [Fig. 5(a)].

Thus, by quenching the spin polarization with a magnetic field, one can unravel the charge-state dynamics of the NV centers during illumination as well as in the dark. We note here that, with the 532-nm laser excitation, in spite of the narrow spectral window chosen there could still be a slight overlap of spectra of the two charge states. However, previous reports suggest that spectral filtering gives reliable quantification of the charge-state ratio in an ensemble [44]. The accuracy of quantification of the charge-state distribution could be improved by selective excitation of the NV^{0} and NV^{-} centers by a blue and red laser, respectively [16], instead of green excitation.

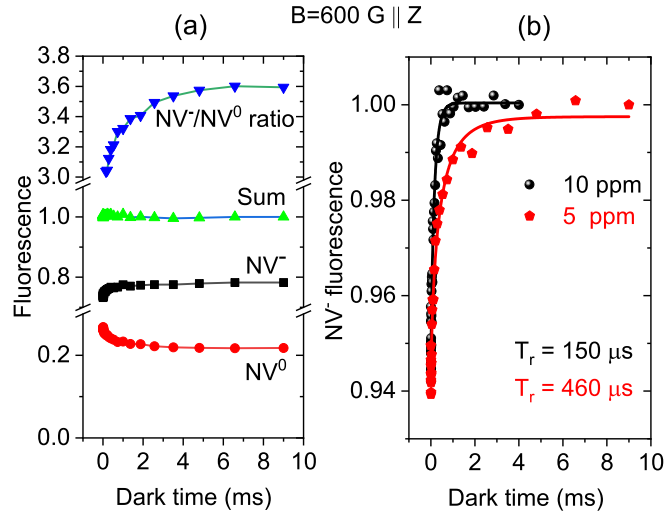

FIG. 5. (a) Charge-state dynamics of NV centers in nanodiamonds (FND100) in the dark. Charge-state ratio, R, increases as the NV ensemble establishes equilibrium. (b) Effect of NV density (5 vs 10 ppm) on the recharging time. The recharge-in-the-dark process becomes faster with increasing NV density.

As a possible application to understand the physical mechanisms governing charge-state instability, we applied this technique to two systems.

(i) Ensembles of NV centers in NDs. We compared the charge dynamics in the dark in two ND powder samples, measured at 600 G $\parallel Z$ using the T_1 sequence of Fig. 4(a). The nominal diameter of the NDs is 100 nm. The primary difference between the two samples is the NV densities (one with 5 ppm and the other with 10 ppm of NV centers). The fluorescence intensity increased with dark time, reaching saturation (see Fig. 5). We can interpret this as follows. During illumination NV^{-}'s are ionized increasing the populations of NV^{0}'s [Fig. 2(c)]. In the dark, the NV^{0} centers recharge due to electrons tunneling between proximate NV centers [13], or between NVs and nitrogen impurities [16], and establish a charge equilibrium condition. Thus NV^{-} is the stable charge state in the NDs, despite the large surface area in which the electron traps are known to favor the NV^{0} charge state [45]. Increasing the NV density results in a shorter recharging time, indicating more charge-state instability. This behavior could be due to an increase in the tunneling rates as the distance between the NV centers as well as between NVs and other defects decrease with increasing defect density [46].

(ii) Bulk vs near-surface NV centers in bulk single crystal diamond. Recent work on single NV centers suggests different charge-state dynamics for bulk and near-surface NV centers under green illumination [44]. Here, we show that even in the case of ensembles of NVs, charge-state dynamics of bulk- and the near-surface NV centers are different, both under green illumination as well as in the dark. Near-surface NV centers in a nitrogen-implanted electronic grade CVD sample (EG6), and bulk NV centers from a nonelectronic grade CVD sample (S6) were chosen for the study. We applied a magnetic field of 600 G along the [100] crystallographic direction to

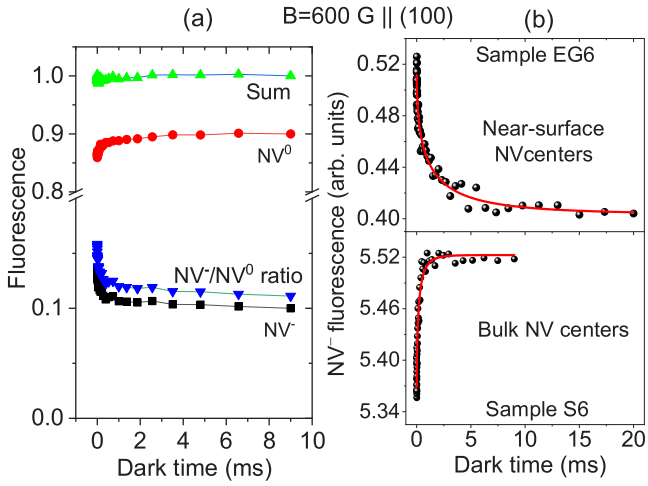

FIG. 6. (a) Charge-state dynamics of the near-surface NV centers (EG6) in the dark. The charge-state ratio, R, decreases with time indicating NV^0 is the preferred charge state. (b) Comparison of charge dynamics of near-surface vs bulk NV centers. The sign of fluorescence evolution in the dark is different for bulk and near-surface NV centers, suggesting location-dependent charge dynamics.

quench the spin polarization. The effect of magnetic field on the fluorescence spectra of the NV ensemble in single-crystal diamonds is similar to that observed in nanodiamonds (see the Appendix). We used the T_1 sequence of Fig. 4(a) to investigate the charge dynamics in the dark. In the case of near-surface NV centers, in the dark, the charge-state ratio, R, decreases with time, and in equilibrium, about 90% of the NV centers are in the neutral charge state [Fig. 6(a)]. However, the charge-state ratio in the steady state under green illumination depends strongly on the laser power [44]. With stronger excitation, NV^- populations can be increased substantially, which is reflected in the fluorescence spectra (lower panel, Fig. 7). In the dark, primarily the NV^- centers ionize due to electron loss to nearby traps [26], establishing an equilibrium condition, in which the NV^0 center is the stable charge state [Fig. 6(a)]. This result is a consequence of the fact that the diamond surface is known to favor the neutral charge state [18,47,48]. This result has implications for the use of NV centers in sensing applications, in which an ensemble of near-surface negatively charged NV centers are required. One of the primary factors is the presence of the surface electron traps, and controlling their charge states could improve the stability of the NV^- centers [26]. The dynamics are exactly opposite in the case of bulk NV centers and similar to the NDs, the equilibrium condition is the one in which NV^- is the favored configuration [Fig. 6(b)].

IV. CONCLUSIONS

To summarize, we have shown that it is possible to completely decouple the effect of spin from charge dynamics measurements with an off-axis magnetic field, without substantially affecting their charge-state stability. Our method also allows quantification of the charge-state distribution of an NV ensemble at a given time during laser illumination as well as in the dark. In 100-nm NDs, we demonstrate that despite their large surface area NV^- is the favored charge state both under illumination as well as in the dark, and the charge-state instability scales with the density of NV centers. This observation has direct implications in the use of NDs for sensing applications in biological systems, where highly fluorescent NDs are required. We also show that, in bulk single-crystal diamonds, the charge stability of the NV centers depends on their location in the sample. In the bulk of the diamond, the NV centers are mostly stable in the negative charge state. However, the all-important near-surface NV centers are mostly stable in the undesirable neutral charge state. The nonperturbative technique to study charge-state dynamics we demonstrated here could help better understand charge-state dynamics due to tunneling to defect sites in high NV density nanodiamonds in which the production process can generate high defect concentrations. It could also be useful to investigate the effect of surface states, local charge environments on the charge-state stability. A better understanding of the processes could help to optimize the diamond surface to increase the NV^- populations of the near-surface NV centers.

APPENDIX: FLUORESCENCE SPECTRA OF NV ENSEMBLE IN BULK DIAMOND

The fluorescence emission spectra of the two bulk single-crystal diamonds used in the study are shown in Fig. 7. We used higher laser power (50 mW for S6, and 100 mW for EG6) to acquire the spectra, due to poor sensitivity of the spectrometer. An external magnetic field aligned along the (100) direction makes an equal angle to all four NV orientations (54.7°). With a static magnetic field of 600 G || (100), complete mixing of the spin states is achieved, which quenches the spin polarization. As a consequence, the fluorescence of the NV^- centers (650–800 nm band) decreases. However, the NV^0 emission (575-nm zero-phonon line) is hardly affected, similar to the case of nanodiamonds.

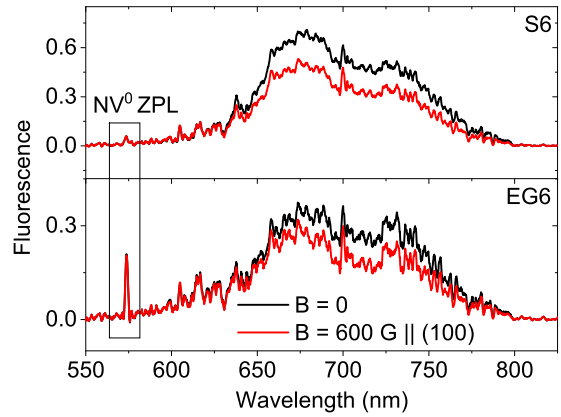

FIG. 7. Effect of a magnetic field. The fluorescence spectra of a NV ensemble in the single-crystal CVD diamonds, with- and without an external magnetic field.

[1] G. Davies and M. F. Hamerand, Proc. R. Soc. London, Ser. A **348**, 285 (1976).

[2] G. Davies, S. C. Lawson, A. T. Collins, A. Mainwood, and S. J. Sharp, Phys. Rev. B **46**, 13157 (1992).

[3] K. Iakoubovskii, G. J. Adriaenssens, and M. Nesladek, J. Phys.: Condens. Matter **12**, 189 (2000).

[4] A. Gruber, A. Drabenstedt, C. Tietz, L. Fleury, J. Wrachtrup, and C. v. Borczyskowski, Science **276**, 2012 (1997).

[5] S. Felton, A. M. Edmonds, M. E. Newton, P. M. Martineau, D. Fisher, and D. J. Twitchen, Phys. Rev. B **77**, 081201(R) (2008).

[6] A. Gali, Phys. Rev. B **79**, 235210 (2009).

[7] F. Dolde, H. Fedder, M. W. Doherty, T. Nöbauer, F. Rempp, G. Balasubramanian, T. Wolf, F. Reinhard, L. C. Hollenberg, F. Jelezko, and J. Wrachtrup, Nat. Phys. **7**, 459 (2011).

[8] L. Childress and R. Hanson, MRS Bull. **38**, 134 (2013).

[9] L. Rondin, J. P. Tetienne, T. Hingant, J. F. Roch, P. Maletinsky, and V. Jacques, Rep. Prog. Phys. **77**, 056503 (2014).

[10] J. P. Tetienne, A. Lombard, D. A. Simpson, C. Ritchie, J. Lu, P. Mulvaney, and L. C. Hollenberg, Nano Lett. **16**, 326 (2016).

[11] S. Karaveli, O. Gaathon, A. Wolcott, R. Sakakibara, O. A. Shemesh, D. S. Peterka, E. S. Boyden, J. S. Owen, R. Yuste, and D. Englund, Proc. Natl. Acad. Sci. USA **113**, 3938 (2016).

[12] M. Pfender, N. Aslam, H. Sumiya, S. Onoda, P. Neumann, J. Isoya, C. A. Meriles, and J. Wrachtrup, Nano Lett. **17**, 5931 (2017).

[13] J. Choi, S. Choi, G. Kucsko, P. C. Maurer, B. J. Shields, H. Sumiya, S. Onoda, J. Isoya, E. Demler, F. Jelezko, N. Y. Yao, and M. D. Lukin, Phys. Rev. Lett. **118**, 093601 (2017).

[14] N. B. Manson and J. P. Harrison, Diam. Relat. Mater. **14**, 1705 (2005).

[15] S. Dhomkar, H. Jayakumar, P. R. Zangara, and C. A. Meriles, Nano Lett. **18**, 4046 (2018).

[16] N. B. Manson, M. Hedges, S. Michael, J. Barson, R. Ahlefeldt, M. W. Doherty, H. Abe, T. Ohshima, and M. J. Sellars, New J. Phys. **20**, 113037 (2018).

[17] X. D. Chen, L. M. Zhou, C. L. Zou, C. C. Li, Y. Dong, F. W. Sun, and G. C. Guo, Phys. Rev. B **92**, 104301 (2015).

[18] M. V. Hauf, B. Grotz, B. Naydenov, M. Dankerl, S. Pezzagna, J. Meijer, F. Jelezko, J. Wrachtrup, M. Stutzmann, F. Reinhard, and J. A. Garrido, Phys. Rev. B **83**, 081304(R) (2011).

[19] B. Grotz, M. V. Hauf, M. Dankerl, B. Naydenov, S. Pezzagna, J. Meijer, F. Jelezko, J. Wrachtrup, M. Stutzmann, F. Reinhard, and J. A. Garrido, Nat. Commun. **3**, 729 (2012).

[20] Y. Doi, T. Makino, H. Kato, D. Takeuchi, M. Ogura, H. Okushi, H. Morishita, T. Tashima, S. Miwa, S. Yamasaki, P. Neumann, J. Wrachtrup, Y. Suzuki, and N. Mizuochi, Phys. Rev. X **4**, 011057 (2014).

[21] M. Shimizu, T. Makino, T. Iwasaki, K. Tahara, H. Kato, N. Mizuochi, S. Yamasaki, and M. Hatano, Appl. Phys. Express **11**, 033004 (2018).

[22] T. Murai, T. Makino, H. Kato, M. Shimizu, T. Murooka, E. D. Herbschleb, Y. Doi, H. Morishita, M. Fujiwara, M. Hatano, S. Yamasaki, and N. Mizuochi, Appl. Phys. Lett. **112**, 111903 (2018).

[23] H. Jayakumar, J. Henshaw, S. Dhomkar, D. Pagliero, A. Laraoui, N. B. Manson, R. Albu, M. W. Doherty, and C. A. Meriles, Nat. Commun. **7**, 12660 (2016).

[24] S. Dhomkar, J. Henshaw, H. Jayakumar, and C. A. Meriles, Sci. Adv. **2**, e1600911 (2016).

[25] R. Giri, F. Gorrini, C. Dorigoni, C. E. Avalos, M. Cazzanelli, S. Tambalo, and A. Bifone, Phys. Rev. B **98**, 045401 (2018).

[26] D. Bluvstein, Z. Zhang, and A. C. Bleszynski Jayich, Phys. Rev. Lett. **122**, 076101 (2019).

[27] A. Jarmola, V. M. Acosta, K. Jensen, S. Chemerisov, and D. Budker, Phys. Rev. Lett. **108**, 197601 (2012).

[28] B. A. Myers, A. Ariyaratne, and A. C. Bleszynski Jayich, Phys. Rev. Lett. **118**, 197201 (2017).

[29] D. A. Hopper, R. R. Grote, S. M. Parks, and L. C. Bassett, ACS Nano **12**, 4678 (2018).

[30] N. Aslam, G. Waldherr, P. Neumann, F. Jelezko, and J. Wrachtrup, New J. Phys. **15**, 13064 (2013)

[31] D. P. L. Aude Craik, P. Kehayias, A. S. Greenspon, X. Zhang, M. J. Turner, J. M. Schloss, E. Bauch, C. A. Hart, E. L. Hu, and R. L. Walsworth, arXiv:1811.01972.

[32] R. J. Epstein, F. M. Mendoza, Y. K. Kato, and D. D. Awschalom, Nat. Phys. **1**, 94 (2005).

[33] N. D. Lai, D. Zheng, F. Jelezko, F. Treussart, and J. F. Roch, Appl. Phys. Lett. **95**, 133101 (2009).

[34] J. P. Tetienne, L. Rondin, P. Spinicelli, M. Chipaux, T. Debuisschert, J. F. Roch, and V. Jacques, New J. Phys. **14**, 103033 (2012).

[35] J. Ziegler, The Stopping Range of Ions in Matter, SRIM-2008, http://www.srim.org/

[36] P. Ji and M. V. Gurudev Dutt, Phys. Rev. B **94**, 024101 (2016).

[37] M. Capelli, P. Reineck, D. W. M. Lau, A. Orth, J. Jeske, M. W. Doherty, T. Ohshima, A. D. Greentree, and B. C. Gibson, Nanoscale **9**, 9299 (2017).

[38] N. B. Manson, J. P. Harrison, and M. J. Sellars, Phys. Rev. B **74**, 104303 (2006).

[39] X. D. Chen, C. L. Zou, F. W. Sun, and G. C. Guo, Appl. Phys. Lett. **103**, 013112 (2013).

[40] J. Chen, S. Lourette, K. Rezai, T. Hoelzer, M. Lake, M. Nesladek, L. S. Bouchard, P. Hemmer, and D. Budker, Appl. Phys. Lett. **110**, 011108 (2017).

[41] I. N. Kupriyanov, V. A. Gusev, N. P. Yu, and M. B. Yu, J. Phys.: Condens. Matter **12**, 7843 (2000).

[42] T. Gaebel, M. Domhan, C. Wittmann, I. Popa, F. Jelezko, J. Rabeau, A. Greentree, S. Prawer, E. Trajkov, P. R. Hemmer, and J. Wrachtrup, Appl. Phys. B **82**, 243 (2005).

[43] F. Gorrini, R. Giri, C. E. Avalos, S. Tambalo, S. Mannucci, L. Basso, N. Bazzanella, C. Dorigoni, M. Cazzanelli, P. Marzola, A. Miotello, and A. Bifone, arXiv:1808.03525.

[44] I. Meirzada, Y. Hovav, S. A. Wolf, and N. Bar-Gill, Phys. Rev. B **98**, 245411 (2018).

[45] L. Rondin, G. Dantelle, A. Slablab, F. Grosshans, F. Treussart, P. Bergonzo, S. Perruchas, T. Gacoin, M. Chaigneau, H. C. Chang, V. Jacques, and J. F. Roch, Phys. Rev. B **82**, 115449 (2010).

[46] J. P. Chou, Z. Bodrog, and A. Gali, Phys. Rev. Lett. **120**, 136401 (2018).

[47] C. Santori, P. E. Barclay, K.-M. C. Fu, and R. G. Beausoleil, Phys. Rev. B **79**, 125313 (2009).

[48] K. M. C. Fu, C. Santori, P. E. Barclay, and R. G. Beausoleil, Appl. Phys. Lett. **96**, 121907 (2010).